1

ARMY RESEARCH LABORATORY

A Computational Study of Detonation Failure in Composition B and Cast TNT Charges

John Starkenberg
Toni M. Dorsey

ARL-TR-616

November 1994

NOTICES

REPORT DOCUMENTATION PAGE

Form Approved
OMB No 0704-0188

1. AGENCY USE ONLY *(Leave blank)*

2. REPORT DATE
November 1994

3. REPORT TYPE AND DATES COVERED
Final, 1 October 1992–30 April 1994

4. TITLE AND SUBTITLE
A Computational Study of Detonation Failure in Composition B and Cast TNT Charges

5. FUNDING NUMBERS
PR: 1L162618AH80

6. AUTHOR(S)
John Starkenberg and Toni M. Dorsey

7. PERFORMING ORGANIZATION NAME(S) AND ADDRESS(ES)
U.S. Army Research Laboratory
ATTN: AMSRL-WT-TB
Aberdeen Proving Ground, MD 21005-5066

8. PERFORMING ORGANIZATION REPORT NUMBER

9. SPONSORING / MONITORING AGENCY NAME(S) AND ADDRESS(ES)
U.S. Army Research Laboratory
ATTN: AMSRL-OP-AP-L
Aberdeen Proving Ground, MD 21005-5066

10. SPONSORING / MONITORING AGENCY REPORT NUMBER
ARL-TR-616

11. SUPPLEMENTARY NOTES

12a. DISTRIBUTION / AVAILABILITY STATEMENT
Approved for public release; distribution is unlimited.

12b. DISTRIBUTION CODE

13. ABSTRACT *(Maximum 200 words)*

In order to obtain a broader understanding of the utility of the Forest Fire explosive initiation model in predicting detonation failure, we made computations using the 2DE code to predict failure diameter and thickness for Composition B and cast TNT. The computations reveal oscillatory detonations near the failure dimension. The computed failure radius is nearly equal to the corresponding failure thickness. The predictions are accurate for Composition B and reasonably close for cast TNT. We also made 2DE computations of detonation failure in singly perforated grains of each explosive using Forest Fire. For these grains, detonation fails when the failure thickness exceeds the difference between the grain and perf radii. Consideration of the expected behavior when failure radius and thickness are not equal leads to the conclusion that sensitivity of perfed grains is lowest in materials for which failure radius exceeds failure thickness.

14. SUBJECT TERMS
explosives, detonation, critical diameter

15. NUMBER OF PAGES
36

16. PRICE CODE

17. SECURITY CLASSIFICATION OF REPORT	**18. SECURITY CLASSIFICATION OF THIS PAGE**	**19. SECURITY CLASSIFICATION OF ABSTRACT**	**20. LIMITATION OF ABSTRACT**
UNCLASSIFIED	UNCLASSIFIED	UNCLASSIFIED	UL

INTENTIONALLY LEFT BLANK.

ACKNOWLEDGMENT

The authors are grateful to Mrs. Kelly Benjamin for her assistance in insuring that the computations were properly initialized and for preparing some of the final figures for this report.

INTENTIONALLY LEFT BLANK.

TABLE OF CONTENTS

INTENTIONALLY LEFT BLANK.

LIST OF FIGURES

INTENTIONALLY LEFT BLANK.

LIST OF TABLES

INTENTIONALLY LEFT BLANK.

1. BACKGROUND

It is well known that explosive charges can only sustain detonation when their lateral dimensions are sufficiently large (Campbell and Engelke 1976). When this condition is not met, incipient detonations fail as a result of the effects of rarefactions which encroach upon their reaction zones. Thus, for a particular explosive, a failure diameter may be determined for cylindrical charges and a failure thickness may be determined for laminar charges. Mader (1979) has reported accurate predictions of failure diameter in several explosives using the Forest Fire model in the 2DL and 2DE codes. More recently, Lundstrom (1993) has produced less successful predictions of the failure diameter of Composition B using his modified version of Forest Fire in the SMERF code.

In order to obtain a broader understanding of the utility of Forest Fire in predicting detonation failure, we made computations using the 2DE code to predict failure diameter and thickness for Composition B and cast TNT. These explosives were chosen because they have substantially different reaction rates and failure diameters. Our original intention was to include PBX-9404, which has a very small failure diameter, as well. This attempt was abandoned because we encountered too many computational failures.

It has been suggested that propellant grains having perforations, or perfs, might be designed such that they could not sustain detonation even with grain diameters above the failure diameter. For negligibly small perfs, the grain diameter is expected to control failure. However, for sufficiently large perfs in sufficiently large grains, the thickness of the web of solid propellant between perfs may control failure.

In an attempt to shed some light on this question, we made 2DE computations of detonation failure in singly perforated (axisymmetric) grains of Composition B and cast TNT modeled using Forest Fire.

2. DESCRIPTION OF 2DE AND FOREST FIRE

The 2DE Code is a two-dimensional Eulerian finite-difference solver for the continuum mechanics conservation equations (Mader 1970; Kershner and Mader 1972). It was developed at the Los Alamos Scientific National Laboratory for application to explosive initiation problems. It makes use of the HOM equation of state, the C-J Volume Burn model for detonation propagation and the Forest Fire explosive initiation model (Mader 1970, 1979; Mader and Forest 1976; Lundstrom 1988), which may also be used for detonation propagation. Chemical reaction is described by a single reaction progress variable, the unreacted mass fraction, which varies from one in the unreacted state to zero in the completely reacted state. Shock and detonation waves are treated using the method of artificial viscosity with linear artificial viscosity rather than the quadratic form commonly employed for shock stabilization.

The HOM equation of state gives pressure and temperature as functions of specific volume and internal energy. The shock Hugoniot provides a set of reference states for solid materials while the isentrope emanating from the Chapman-Jouget (C-J) state is used for explosive products. The reference pressures, internal energies, and temperatures are approximated by polynomials of as many as fifteen terms in the logarithm of volume. For two-phase mixtures of reactants and products, conditions of mechanical and thermal equilibrium are enforced. That is, the equations of state are employed in iterative fashion until the phase pressures and temperatures are equal. The thermal equilibrium condition is generally considered inappropriate because of the short times required for explosive reaction. While the consequences of this assumption have been reported to be negligible (Johnson, Tang, and Forest 1985; Wackerle and Anderson 1984), we have recently shown that this is not generally true (Starkenberg 1993).

Forest Fire is a reaction rate model that predicts the response of explosives to loading by sustained shock waves. The reaction rate is given as a function of the pressure. The model is empirical and relates each explosive's reaction rate to simple sensitivity data characterizing that explosive collected in the wedge test. Wedge test data is typically summarized in a plot of distance of run to detonation as a function of initial shock pressure known as the "Pop plot" (Ramsay and Popolato 1965). Forest Fire is derived so as to reproduce this behavior. In spite of numerous limitations, Forest Fire, as implemented in 2DE, has been shown to be applicable to a surprising variety of problems (Bowman et al. 1981; Cost et al. 1992; Starkenberg et al. 1984). In this implementation, the linear reactive Hugoniot (which is a part of the Forest Fire derivation) is abandoned and the reaction rate is simply integrated through the artificial time scale associated with the viscous shock as well as in the more accurately represented downstream region. For this reason, the level of artificial viscosity affects the accuracy with which 2DE predicts explosive initiation. Reaction is forced to completion when the mass fraction falls below a specified level or when C-J pressure is reached. In applying Forest Fire, it is important to remember that real explosives exhibit modes of initiation in addition to that reflected in the model.

3. SIMULATION DESCRIPTIONS AND TYPICAL RESULTS

We made computations simulating detonation propagation in solid cylindrical, laminar and hollow cylindrical Composition B and cast TNT charges using Forest Fire calibrations obtained some years ago at the Los Alamos Scientific Laboratory. A number of numerical issues pertinent to these computations are discussed in the appendix. The length of the charges was fixed in all computations at 10 mm for Composition B and 100 mm for cast TNT. In each computation, the explosive was initiated using a "hot spot" (a region in which the density and internal energy of the explosive are initialized above the C-J values) extending radially across the charge and comprising approximately the first 5% of its length. Initially, the detonation emanating from the hot spot is somewhat overdriven. Its persistence when the appropriate charge dimension is less than the failure value is a function of the amount by which it is overdriven. We have assumed that the modeled charges are sufficiently long and that the hot spot is sufficiently weak that detonation failure generally occurs within the available run.

Visualization of the results is facilitated by plotting contours of reactant mass fraction at various times. These plots also show the interfaces between the air, solid explosive and reaction products. Detonation is identified where mass fraction contours corresponding to complete reaction lie close together. When detonation fails, the mass fraction contours spread.

In order to determine failure diameters, we made axisymmetric computations of a cylindrical region in space having equal radius and length. The configuration is illustrated in Figure 1. The explosive lies in the central portion of the region along the horizontal axis, while the outer portion is filled with air.

Sequences of mass fraction contour plots for typical cases showing propagation and failure are shown in Figures 2 through 5. Figure 2 shows detonation failure in a 4.1-mm-diameter Composition B charge. As the wave propagates, the diameter of the core detonation region decreases and the mass fraction contours spread. Figure 3 shows marginal detonation failure in a 4.2-mm-diameter Composition B charge. The detonation diameter decreases in an oscillatory fashion as evidenced by the shape of the interface between the reacting solid explosive and its products. The frequency of the oscillations increases as the detonation fails. Spreading of the mass fraction contours occurs outside the core region. Figure 4 shows marginal detonation propagation in a 4.4-mm-diameter Composition B charge. The detonation diameter first decreases and then increases. Figure 5 shows detonation propagation in a 5.0-mm Composition B charge. The detonation diameter increases and then remains steady.

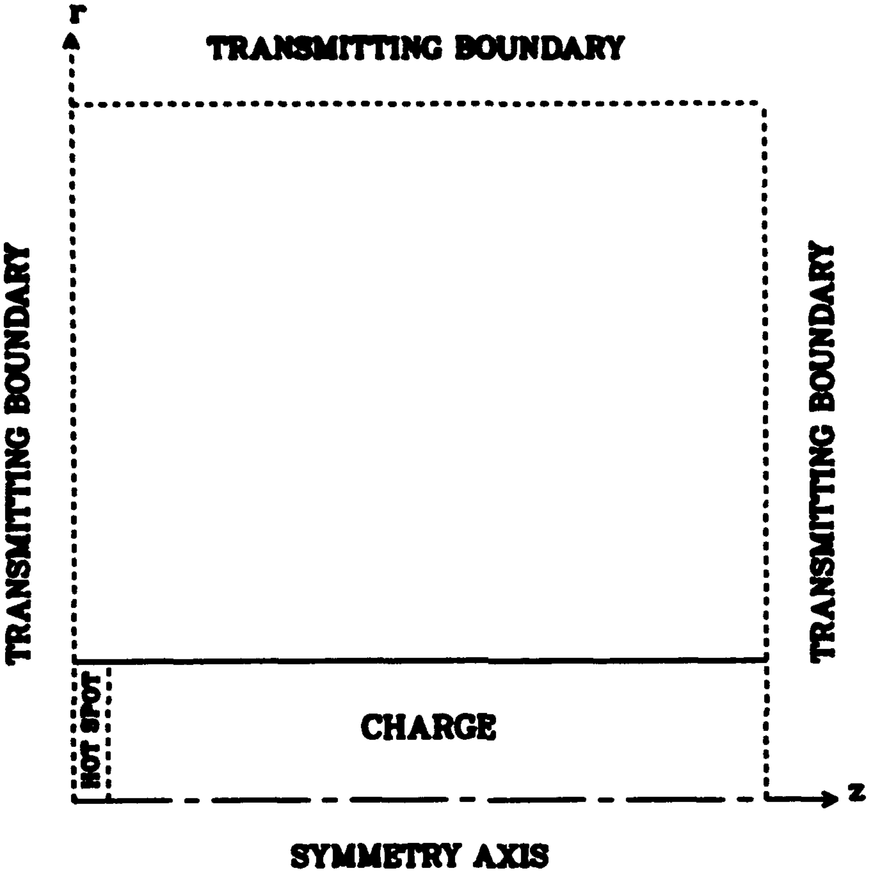

Figure 1. Cylindrical charge computational configuration.

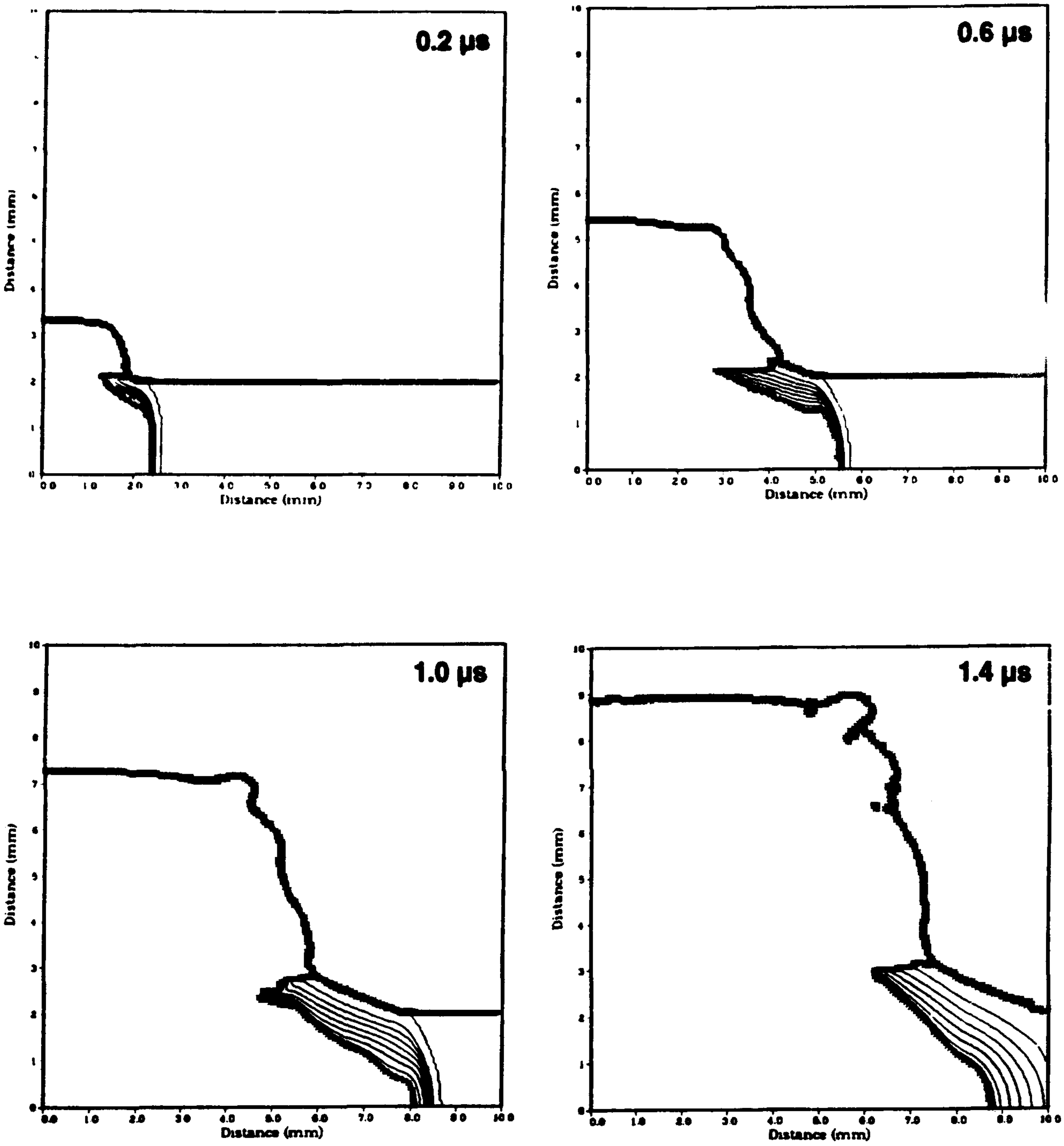

Figure 2. Sequence of mass fraction contour plots showing detonation failure in a 4.1-mm-diameter Composition B charge. The detonation diameter decreases, and the mass fraction contours spread.

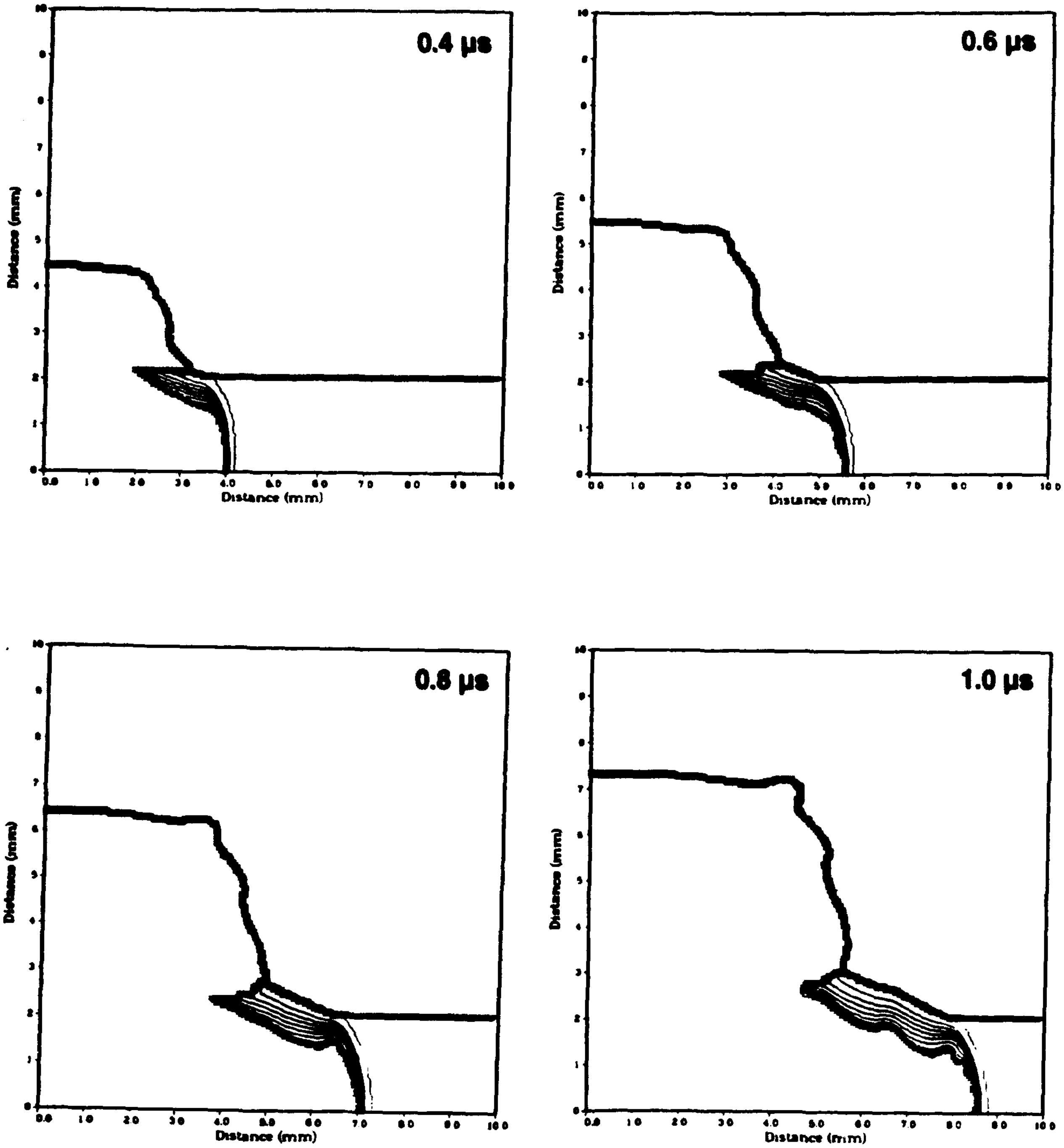

Figure 3. Sequence of mass fraction contour plots showing marginal detonation failure in a 4.2-mm-diameter Composition B charge. The detonation diameter decreases in an oscillatory fashion.

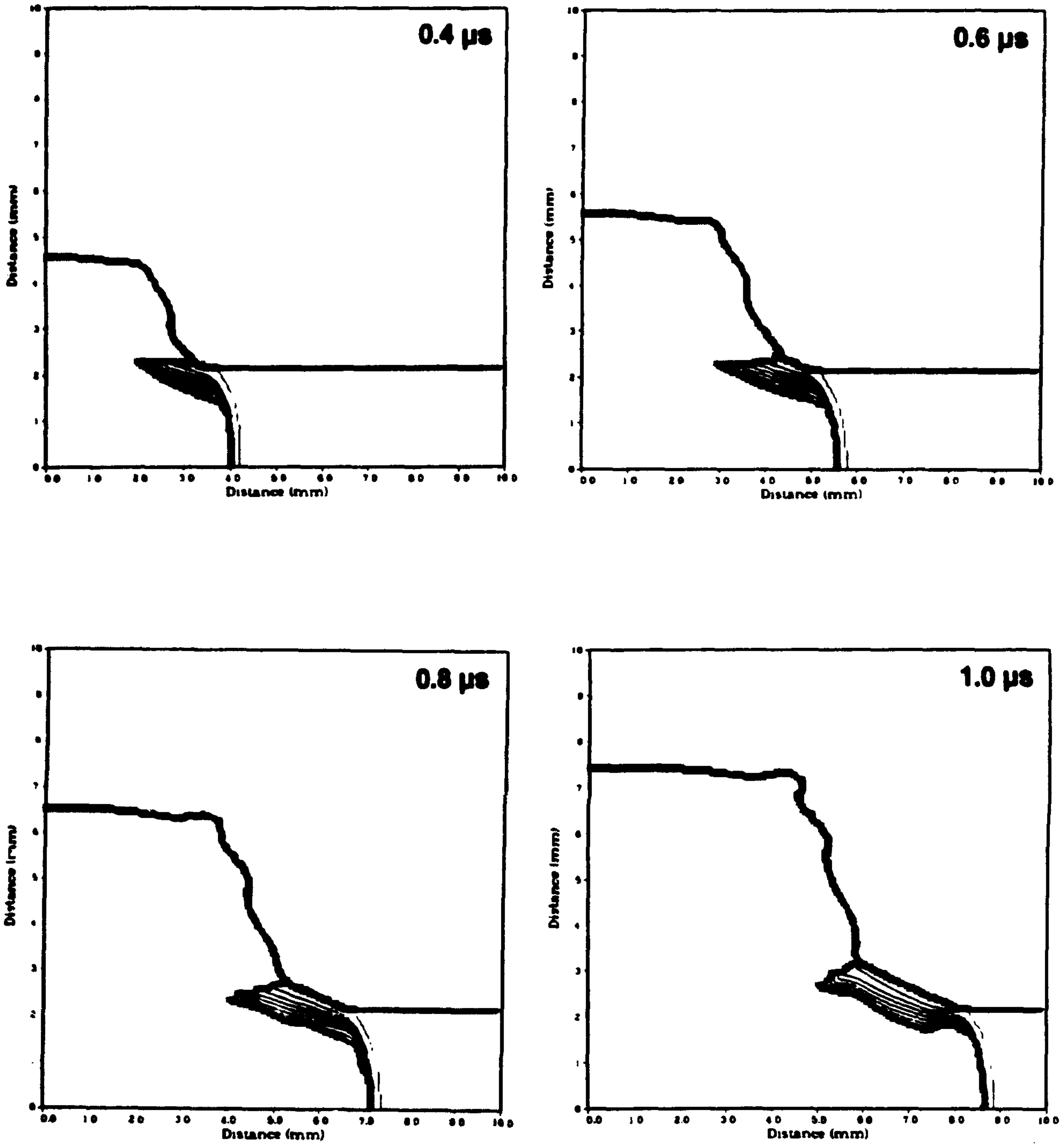

Figure 4. Sequence of mass fraction contour plots showing marginal detonation propagation in a 4.4-mm-diameter Composition B charge. The detonation diameter decreases and then increases.

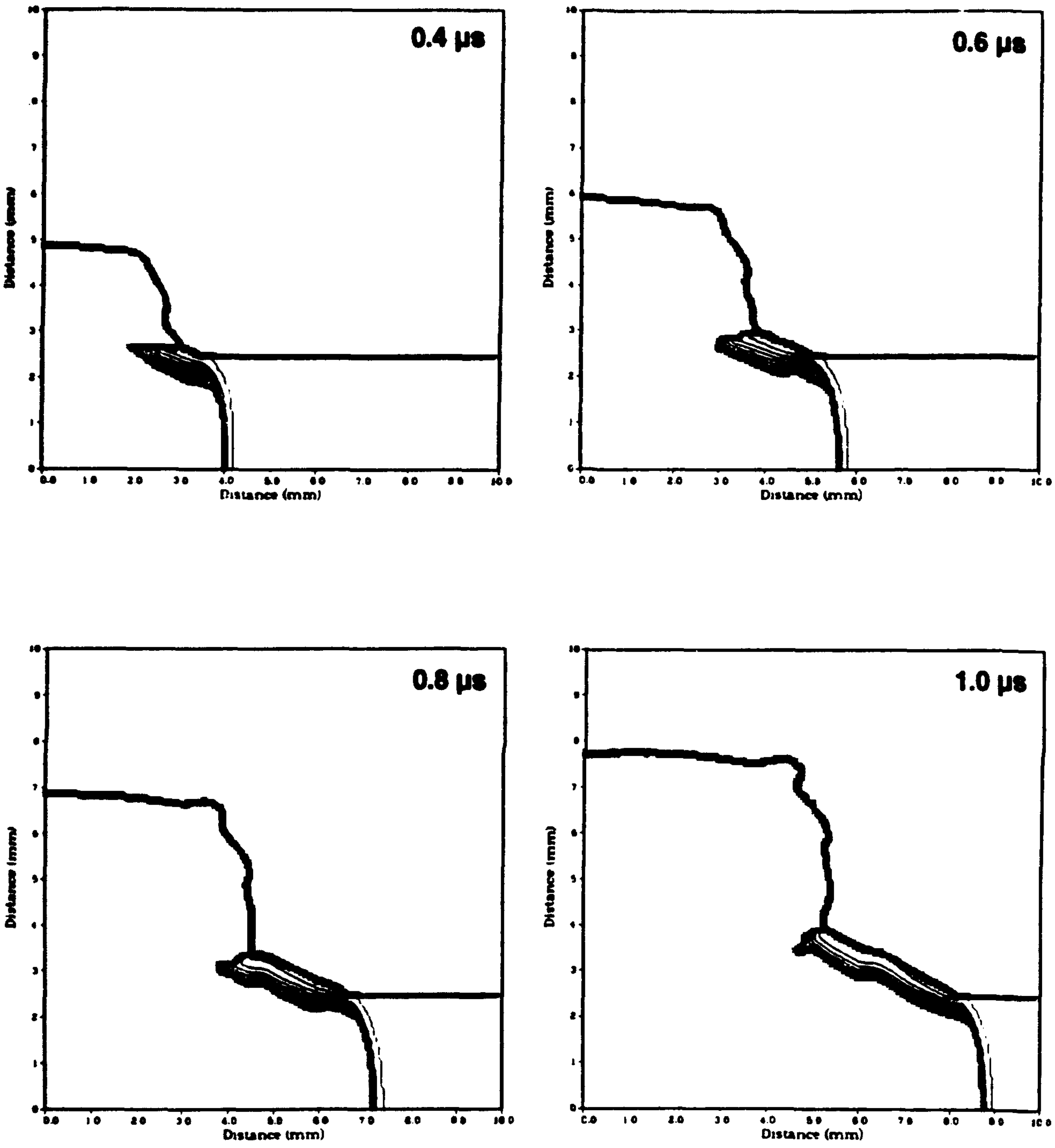

Figure 5. Sequence of mass fraction contour plots showing detonation propagation in a 5.0-mm-diameter Composition B charge. The detonation diameter increases and then remains constant.

For failure thickness determination, we made plane strain computations of a region in space having equal lateral dimensions. The configuration is illustrated in Figure 6. The explosive layer is situated adjacent to a reflective boundary, and the rest of the region is filled with air. Because of the reflective boundary conditions, the reported failure thicknesses are twice the thickness of the computational explosive layer.

Sequences of mass fraction contour plots for typical cases showing propagation and failure are shown in Figures 7 through 9. Figure 7 shows detonation failure in a 2.0-mm-thick Composition B charge. There is some evidence of oscillation of the detonation thickness prior to failure, which occurs after a shorter distance of run than in the axisymmetric case. At late times, propagation of the interface essentially stops. Figure 8 shows marginal detonation propagation for a 2.1-mm-thick Composition B charge. The detonation thickness initially increases, remains constant for a time, and then decreases with evidence of oscillation. This case might fail in a longer charge. Figure 9 shows detonation propagation in a 2.4-mm-thick Composition B charge. The detonation propagates along the charge essentially unchanged.

We represented perforated grains by modifying the axisymmetric configurations used in the failure diameter computations, replacing explosive in the central portion of the cylindrical charge with air. The configuration is illustrated in Figure 10. The radial thickness of the explosive crudely corresponds to the web thickness of more complex grain designs

Sequences of mass fraction contour plots for typical cases showing propagation and failure are shown in Figures 11 and 12. Figure 11 shows detonation failure in a 6.0-mm-diameter Composition B grain with a 1.6-mm-diameter perf. Figure 12 shows marginal detonation propagation with the perf diameter reduced to 1.4 mm. Some oscillation in the detonation is evident.

4. FAILURE RADIUS AND FAILURE THICKNESS

As we shall demonstrate, failure radius is a more convenient parameter than failure diameter for discussion purposes. The computed values of failure radius, r_f, and thickness, h_f, for Composition B and cast TNT are given in Table 1. The computed results are consistent with the simple condition in which the failure radius equals the failure thickness ($r_f = h_f$). The reaction rate is a function of pressure only, and the functional form of the pressure dependence for each explosive is similar. Thus, the ratio of failure radius to failure thickness is governed primarily by hydrodynamic effects.

Table 1. Computed Failure Radii and Thicknesses

Explosive	Failure Radius, r_f (mm)	Failure Thickness, h_f (mm)
Comp B-3	2.10–2.20	2.00–2.20
Cast TNT	16.0–17.0	14.0–16.0

Experimental values of failure radius and thickness for a number of explosives are presented in Table 2. The values for failure radius are taken from Dobratz and Crawford (1985) (where the original source of data for all explosives except Pentolite and cast TNT is Campbell and Engelke [1976]) and for failure thickness from Gibbs and Popolato (1980) (where the original source is Urizar, Peterson, and Smith [1978]). In each case (except for Pentolite), a range of values for failure radius is given. The range for cast TNT is quite large, as data from several sources was used. In contrast, a single value for failure thickness results from the extrapolation used in its determination. We have doubled the values given in the reference to approximate the response of an unconfined layer. Also presented in the table are the ratios of failure radius to failure thickness (which, for Cyclotol, is computed from values for slightly dissimilar formulations). No experimentally determined failure thickness for cast TNT appears to be available.

Table 2. Experimental Failure Radii and Thicknesses

Explosive	Failure Radius, r_f (mm)	Failure Thickness, h_f (mm)	Ratio, r_f/h_f
Comp B-3	1.87–2.12	1.88	0.99–1.13
Cast TNT	6.30–13.7	—	—
Pressed TNT	1.03–1.59	3.84	0.27–0.41
Cyclotol 77/23	2.40–3.60	—	0.79–1.19
Cyclotol 75/25	—	3.02	—
Pentolite	3.35	2.78	1.21
PBX-9404	0.58–0.60	0.92	0.63–0.65

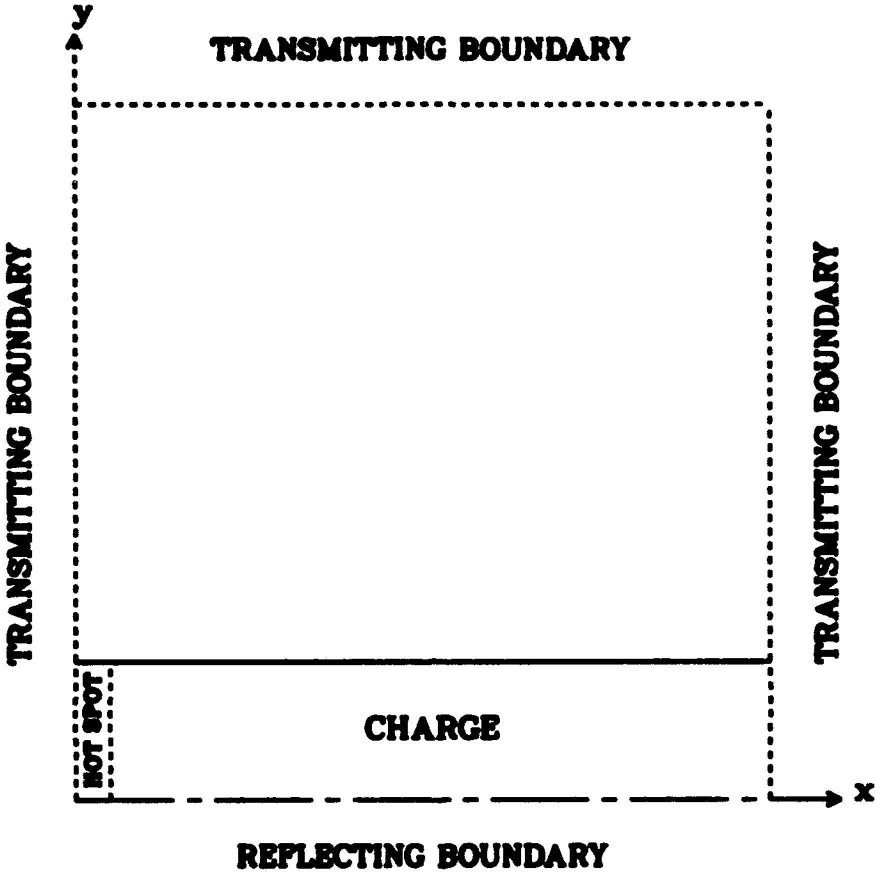

Figure 6. Planar charge computational configuration.

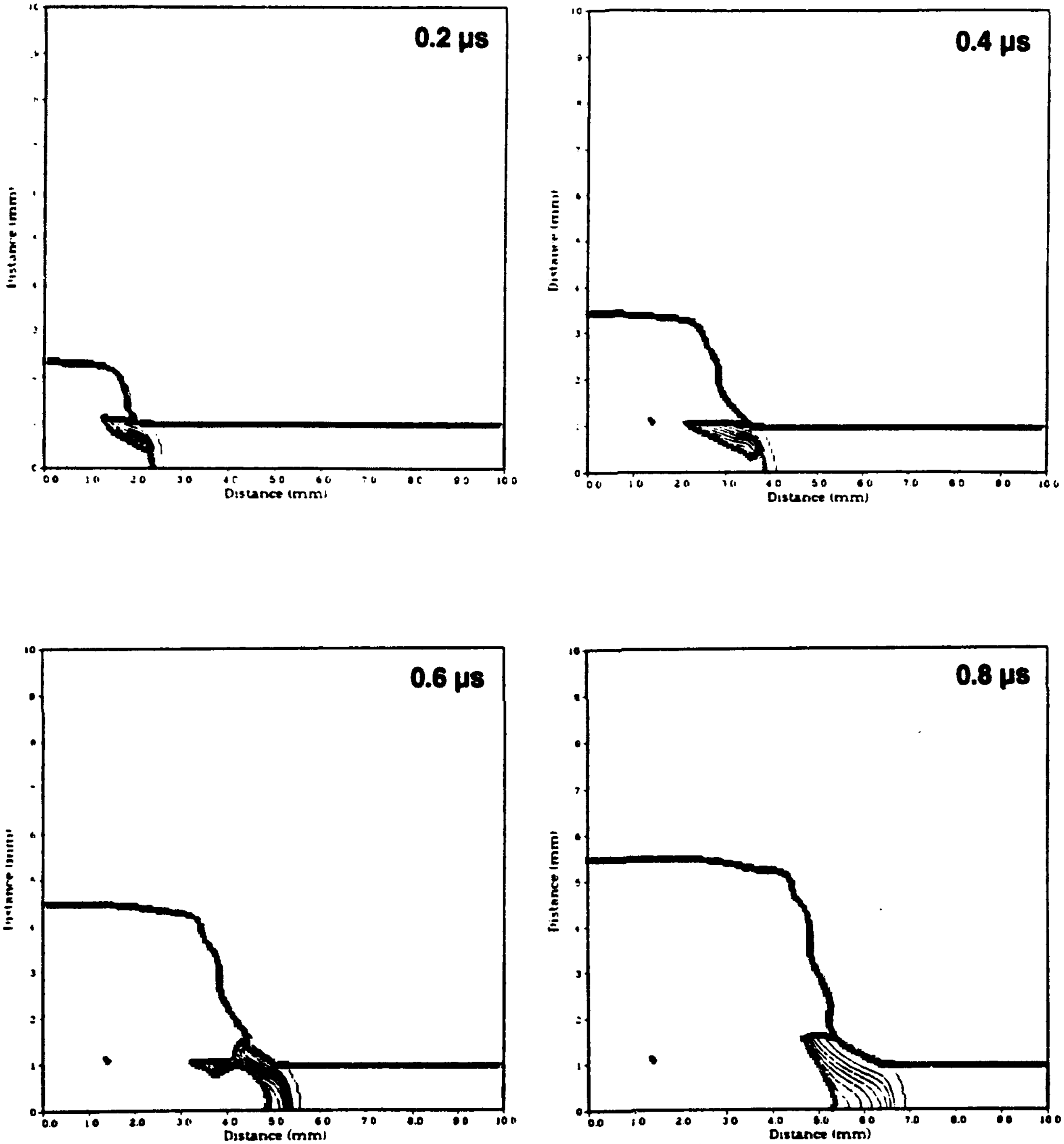

Figure 7. Sequence of mass fraction contour plots showing detonation failure in a 2.0-mm-thick Composition B charge. One oscillation of the detonation thickness occurs before failure, and spreading of the mass fraction contours.

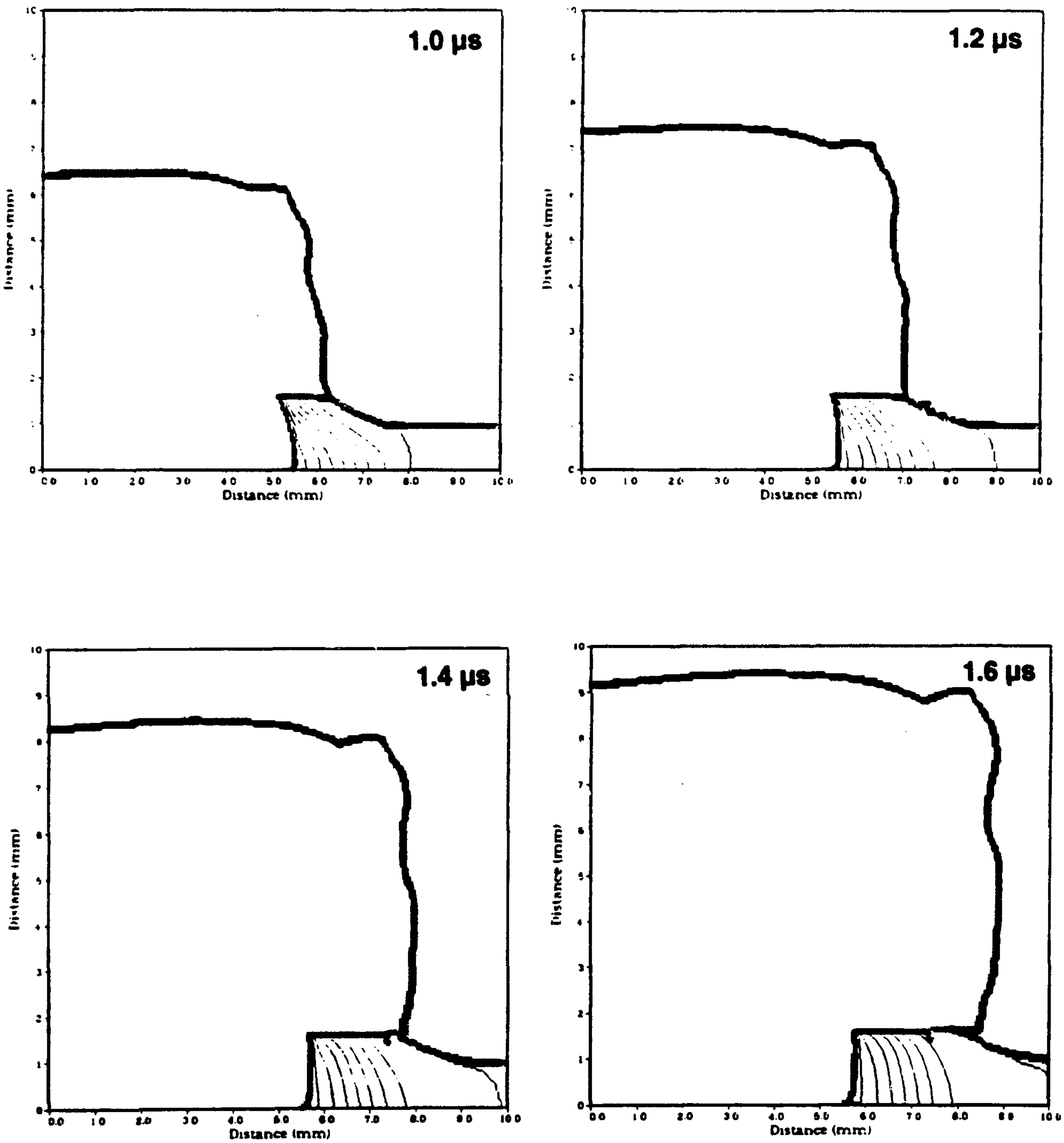

Figure 7. Sequence of mass fraction contour plots showing detonation failure in a 2.0-mm-thick Composition B charge (continued). The mass fraction contours continue to spread, and interface propagation is essentially arrested.

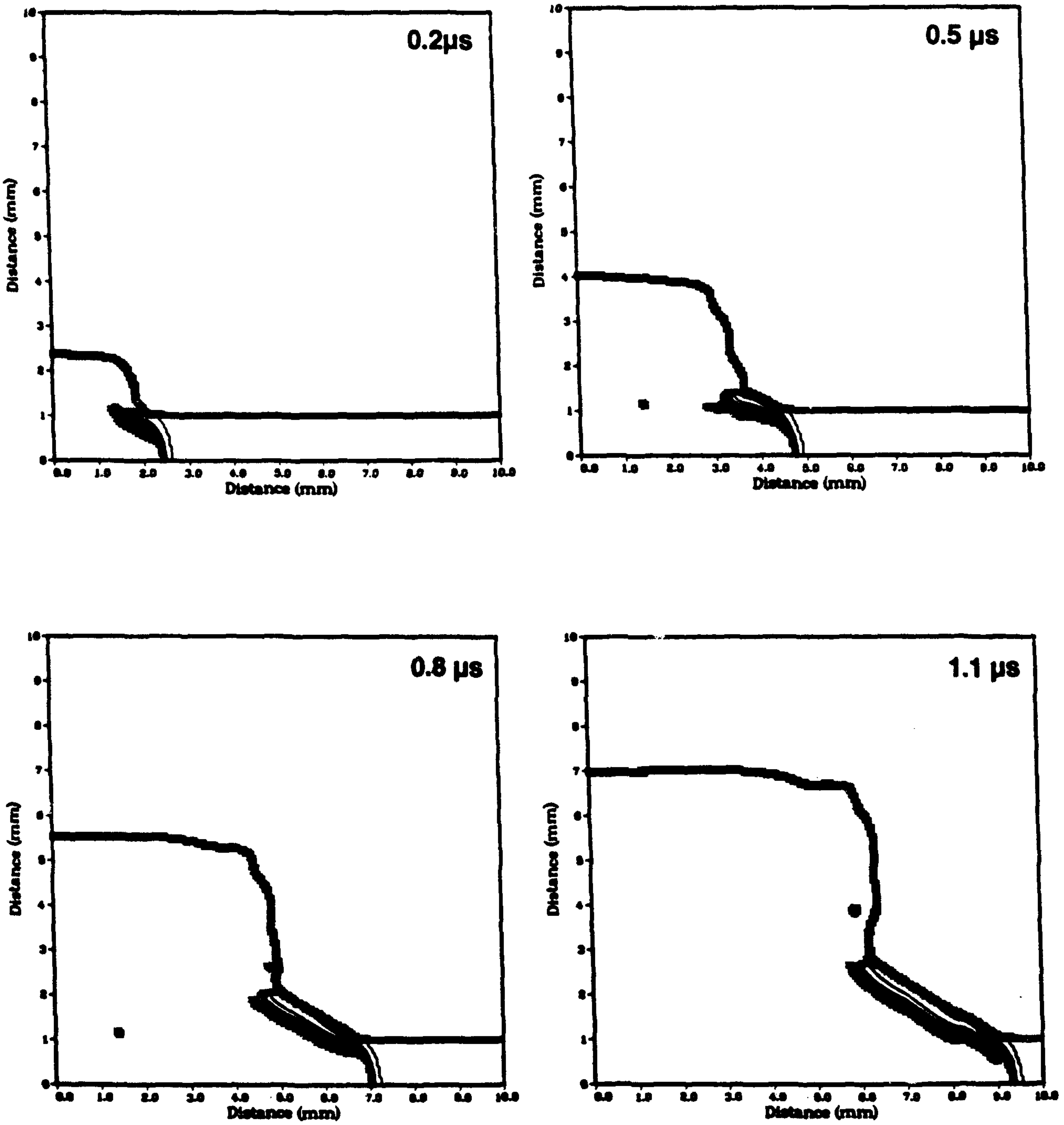

Figure 8. Sequence of mass fraction contour plots showing marginal detonation propagation in a 2.1-mm-thick Composition B charge. The detonation thickness increases before decreasing in an oscillatory fashion.

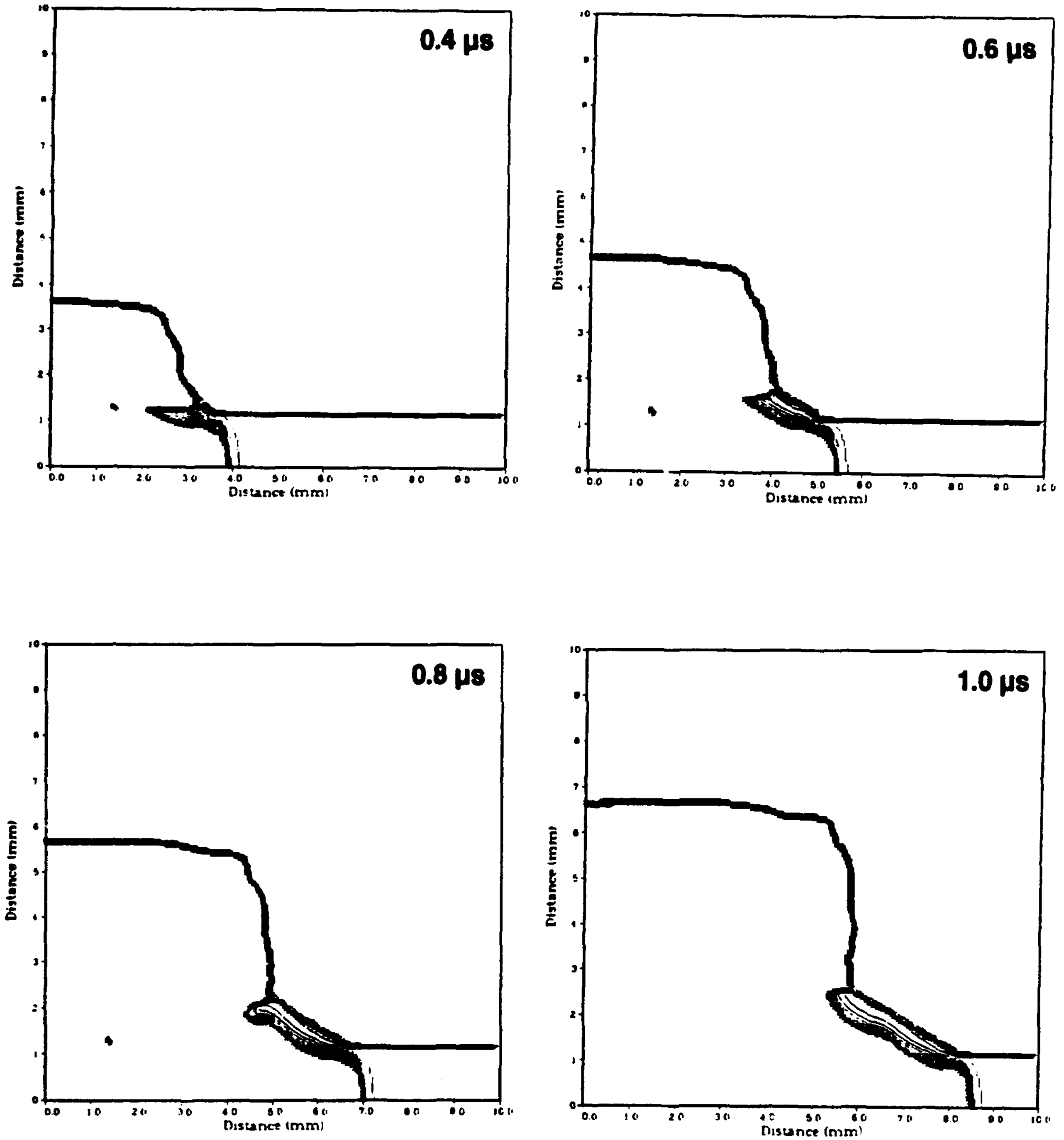

Figure 9. Sequence of mass fraction contour plots showing detonation propagation in a 2.4-mm-thick Composition B charge.

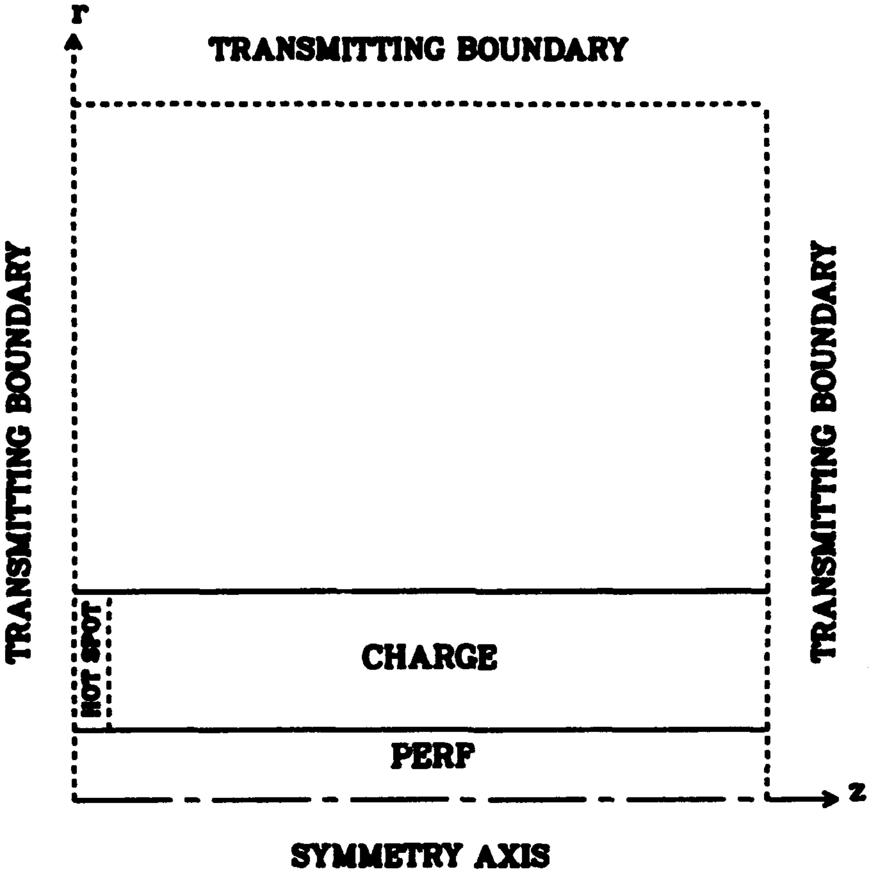

Figure 10. Perfed grain computational configuration.

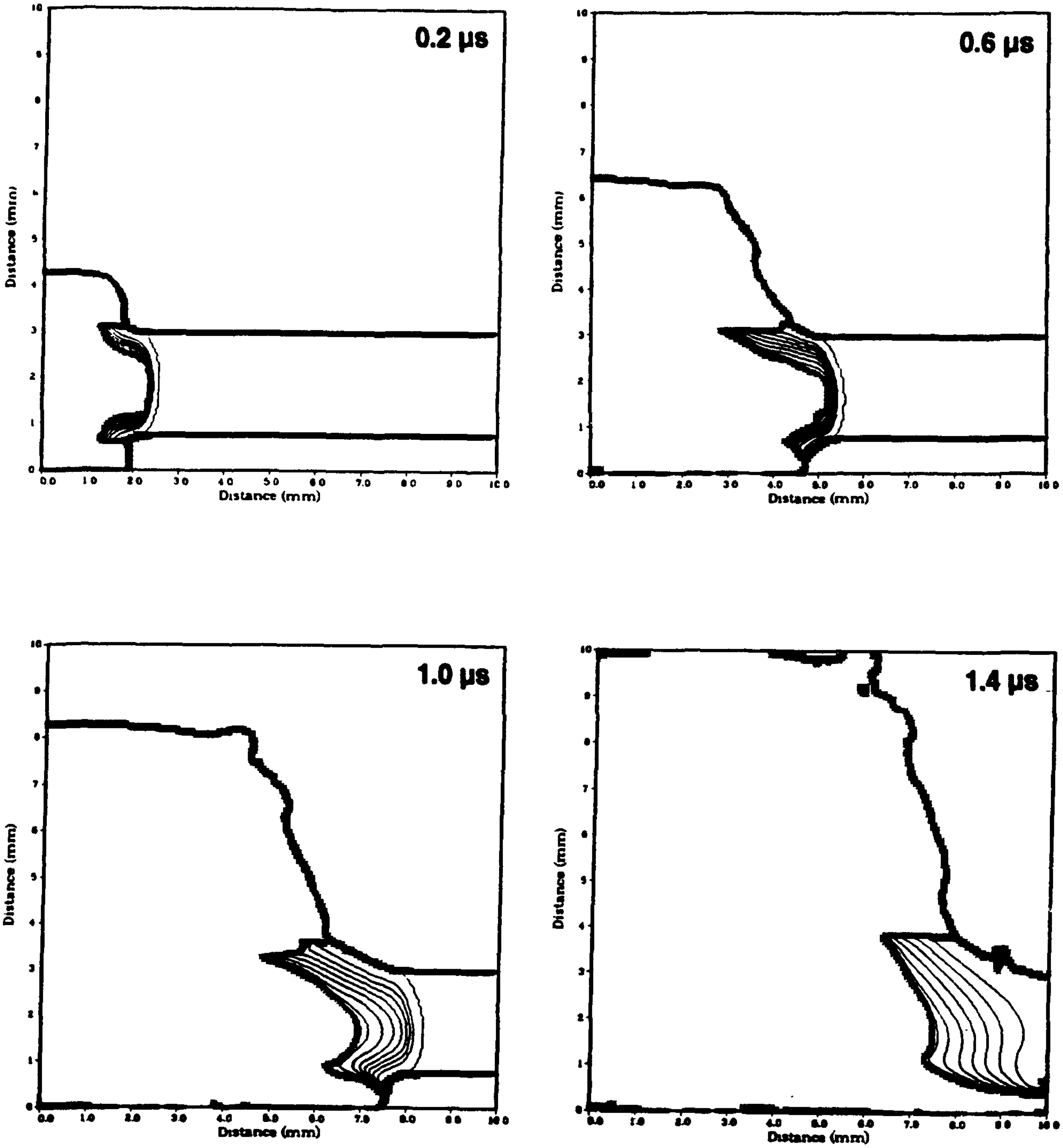

Figure 11. Sequence of mass fraction contour plots showing detonation failure in a 6.0-mm-diameter Composition B grain with a 1.6-mm-diameter perf.

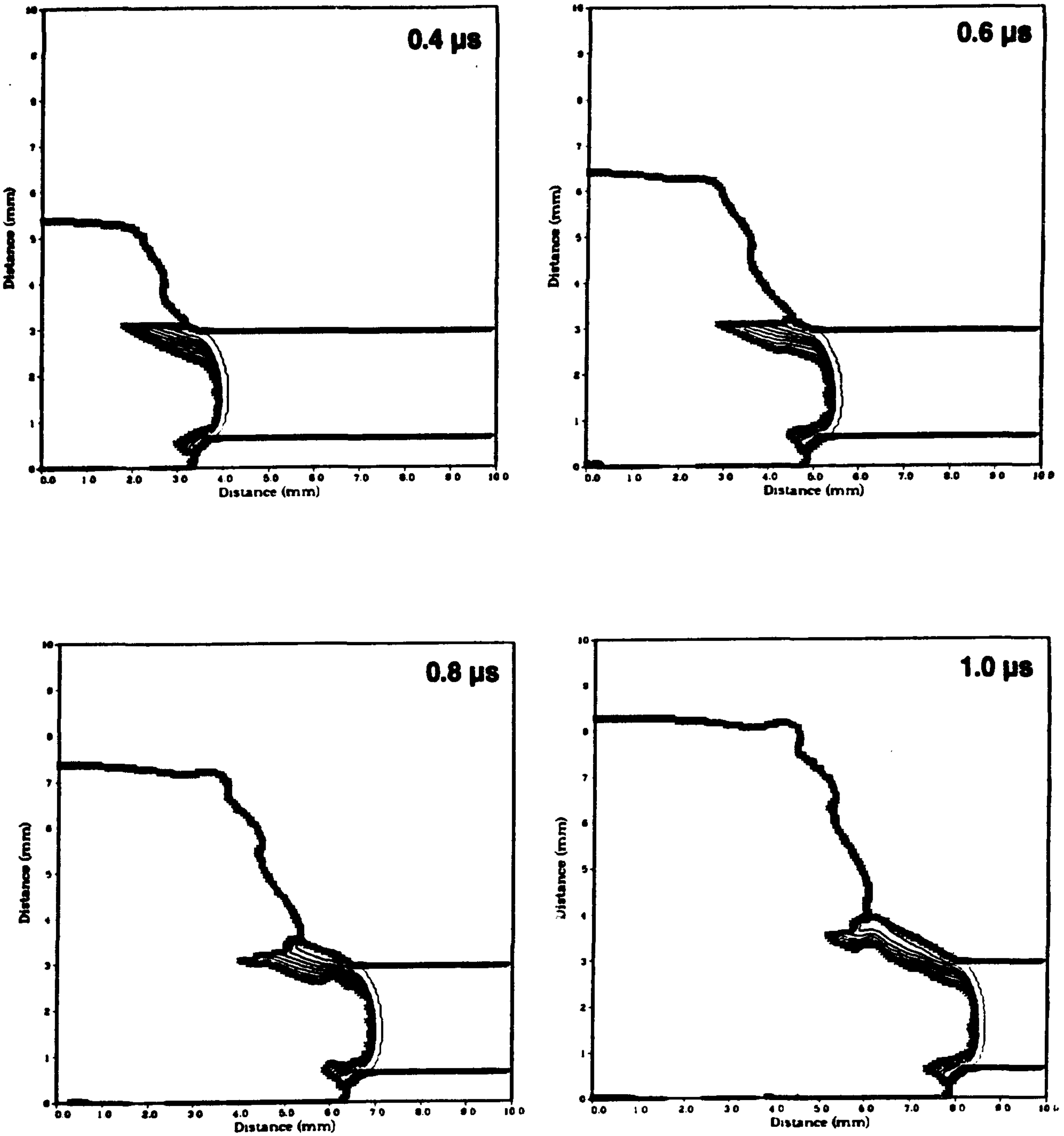

Figure 12. Sequence of mass fraction contour plots showing marginal detonation propagation in a 6.0-mm-diameter Composition B grain with a 1.4-mm-diameter perf. Some oscillation in the detonation is evident.

The computed values for Composition B are close to the experimental values. For cast TNT, the failure radius prediction is reasonably close to the upper limit of the experimental range.

Since the failure radius and failure thickness measurements were made in different places at different times with different batches of explosive, care should be taken in comparing the data. Furthermore, failure thickness is determined by a method which tends to overestimate its value. This is due to the presence of a less than perfectly rigid boundary. Nonetheless, the data indicate that the simple relationship between failure radius and thickness may not be generally applicable. The condition appears to apply to Composition B-3 and, perhaps, Cyclotol, but not to the other explosives listed. Notably, for pressed TNT (if the data are correct), the failure radius is less than half the failure thickness. Consideration of smaller failure thicknesses (to compensate for the overestimation) improves the comparison between failure radius and failure thickness for pressed TNT and PBX-9404, but not for Composition B-3, Cyclotol, or Pentolite.

5. DETONATION FAILURE IN SINGLY PERFORATED GRAINS

Results of computations in which the perf and grain radii of Composition B and cast TNT were varied to determine the critical perf radius as a function of grain radius are shown in Figures 13 and 14. Only results closest to the critical conditions are plotted. In each case, the failure/propagation threshold is defined by the condition, $r_g - r_p = h_f$. That is, the radial ("web") thickness of the explosive layer must exceed the failure thickness in order to sustain detonation. Detonation propagates whenever $r_g - r_p > h_f$ and fails whenever $r_g - r_p < h_f$. No significant effect of layer curvature, even at the smallest diameters, is evident.

This relationship defines "ideal" detonation failure behavior in perfed grains. It is applicable only to materials for which $r_f = h_f$. It is interesting to consider the expected qualitative behavior prevailing for explosives in which the failure radius and failure thickness are not equal. This is illustrated in Figure 15. Here, two curves indicate the critical boundaries associated with failure radii which are respectively greater than and less than the corresponding failure thickness. At large diameters, the failure thickness still controls detonation failure. The shift of the critical boundary associated with energetic materials for which $r_f > h_f$ (if such materials exist) suggests a lower propensity to sustain detonation in perfed grains of these materials.

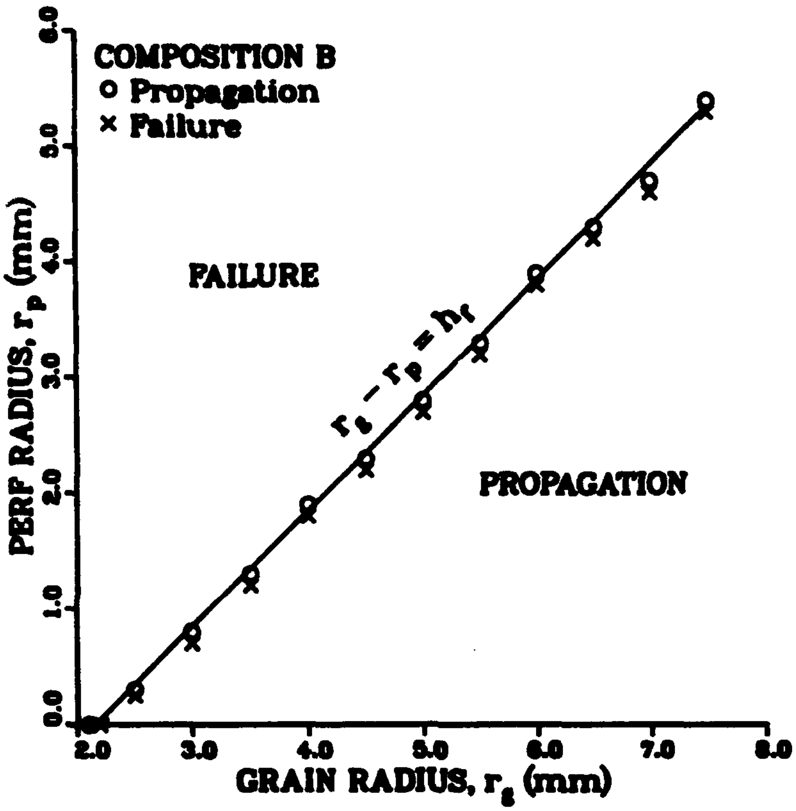

Figure 13. Detonation failure in perfed Composition B grains.

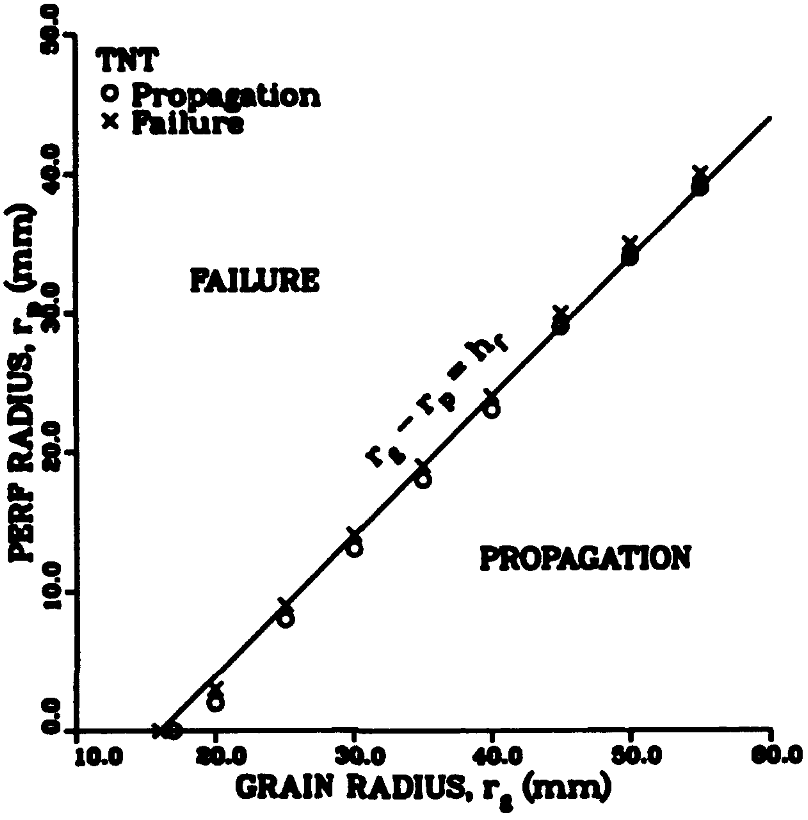

Figure 14. Detonation failure in perfed cast TNT grains.

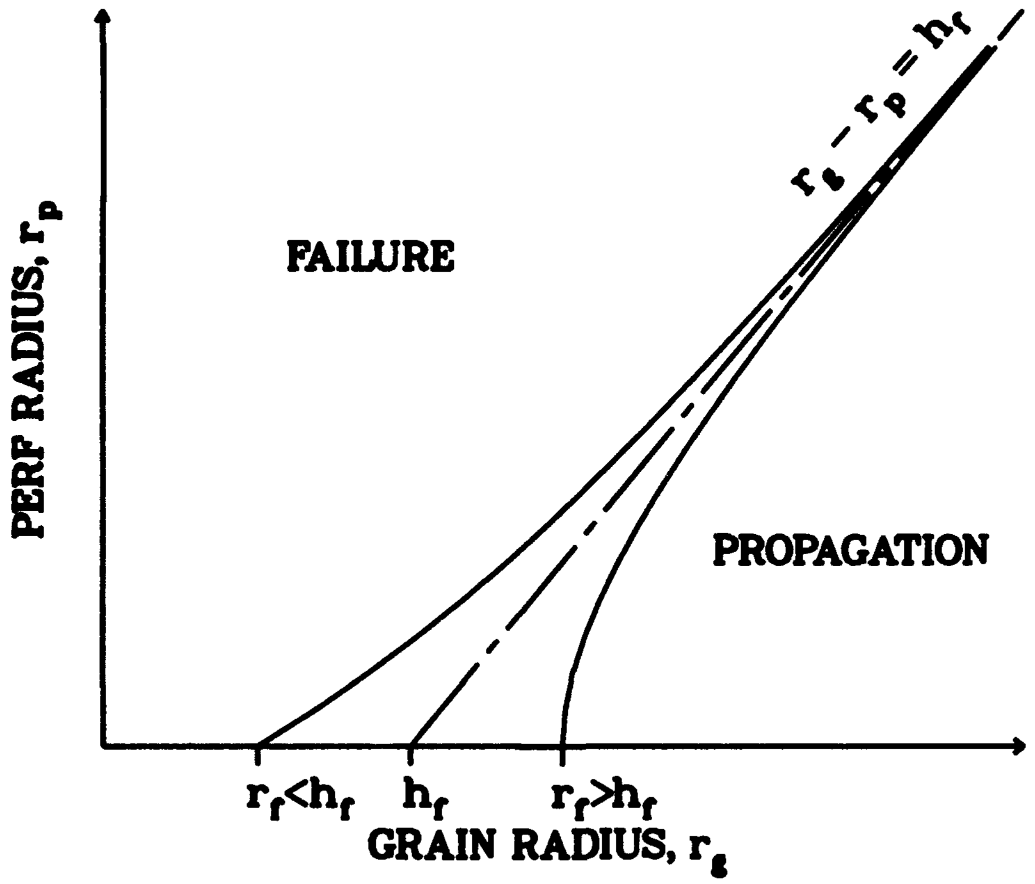

Figure 15. Qualitative detonation failure behavior.

6. SUMMARY AND CONCLUSIONS

2DE predictions of failure diameter and thickness are accurate for Composition B and reasonably close for cast TNT. The computations reveal oscillatory detonations near the failure dimension. The computed failure radius is nearly equal to the corresponding failure thickness. In general, this condition does not appear to hold experimentally.

For perfed grains, detonation fails when the failure thickness exceeds the difference between the grain and perf radii (or radial thickness). If the radial thickness is identified with the web thickness of a more complex grain design, it might be concluded that a sufficient condition for detonation failure in perfed grains is that the failure thickness exceed the web thickness. Consideration of the expected behavior when failure radius and thickness are not equal leads to the conclusion that sensitivity of perfed grains is lowest when failure radius exceeds failure thickness.

While these results are interesting, two problems remain. It is not clear whether energetic materials really exhibit behavior in which the failure radius differs substantially from the failure thickness and, if so, why. Further, the axisymmetric single-perf configuration bears too little resemblance to actual multiple-perf designs to provide useful insight into their behavior. Study of more representative configurations is required for validation of conditions for detonation failure in perfed grains.

INTENTIONALLY LEFT BLANK.

7. REFERENCES

Bowman, A. L., C. A. Forest, J. D. Kershner, C. L. Mader, and G. H. Pimbley. "Numerical Modeling of Shock Sensitivity Experiments." Proceedings of the Seventh Symposium (International) on Detonation, pp. 479–487, 1981.

Campbell, A. W., and R. Engelke. "The Diameter Effect in High-Density Heterogeneous Explosives." Proceedings of the Sixth Symposium (International) on Detonation, pp. 642–652, 1976.

Cost, T. L., W. B. Thomas, S. L. Vance, and D. J. Jones. "Bullet and Fragment Impact Testing and Analysis for the Army IM Database." Proceedings of the 1992 JANNAF Propulsion Systems Hazards Subcommittee Meeting, pp. 227–235, 1992.

Dobratz, B. M., and P. C. Crawford. "LLNL Explosives Handbook." UCRL-52997 Change 2, January 1985.

Gibbs, T. R., and A. Popolato (editors). LASL Explosive Property Data. Berkeley, CA: University of California Press, 1980.

Johnson, J. N., P. K. Tang, and C. A. Forest. "Shock Wave Initiation of Heterogeneous Reactive Solids." Journal of Applied Physics, vol. 57, No. 9, 1985.

Kershner, J. D., and C. L. Mader. "2DE, A Two-Dimensional Continuous Eulerian Hydrodynamic Code for Computing Multicomponent Reactive Hydrodynamic Problems." Report No. LA-4846, Los Alamos Scientific Laboratory, 1972.

Lundstrom, E. A. "Evaluation of Forest Fire Burn Model of Reaction Kinetics of Heterogeneous Explosives." Naval Weapons Center Technical Publication 6898, 1988.

Lundstrom, E. A. "A Numerical Study of Fragment Impact on Bare Explosive." Proceedings of the 1993 JANNAF Propulsion Systems Hazards Subcommittee Meeting, 1993.

Mader, C. L. "An Empirical Model of Heterogeneous Shock Initiation of 9404." Report No. LA-4475, Los Alamos Scientific Laboratory, 1970.

Mader, C. L. Numerical Modeling of Detonation, Berkeley CA: University of California Press, 1979.

Mader, C. L., and C. A. Forest. "Two Dimensional Homogeneous and Heterogeneous Detonation Wave Propagation." Report No. LA-6259, Los Alamos Scientific Laboratory, 1976.

Ramsay, J. B., and A. Popolato. "Analysis of Shock Wave and Initiation Data for Solid Explosives." Proceedings of the Fourth Symposium (International) on Detonation, pp. 233–238, 1965.

Starkenberg, J., Y. K. Huang, and A. L. Arbuckle. "Numerical Modeling of Projectile Impact Shock Initiation of Bare and Covered Composition B." BRL-TR-02576, U.S. Army Ballistic Research Laboratory, Aberdeen Proving Ground, MD, 1984.

Starkenberg, J. "An Assessment of the Performance of the Original and Modified Versions of the Forest Fire Explosive Initiation Model." Proceedings of the Tenth International Detonation Symposium, 1993.

Urizar, M. J., S. W. Peterson, and L. C. Smith. "Detonation Sensitivity Tests." Report LA-7193-MS, Los Alamos Scientific Laboratory, 1978.

Wackerle, J., and A. B. Anderson. "Burning Topology in the Shock-Induced Reaction of Heterogeneous Explosives, Shock Waves in Condensed Matter." J. R. Asay, R. A. Graham, G. K. Straub (eds.), Elsevier Science Publishers B. V., 1984.

APPENDIX:

NUMERICAL CONSIDERATIONS

INTENTIONALLY LEFT BLANK.

EFFECTS OF ARTIFICIAL VISCOSITY

Artificial viscosity provides a method for representing a thin shock wave in a computational grid which is much too coarse to resolve the shock on its actual scale. When too little artificial viscosity is prescribed, large overshoots in the shock pressure result. Since the Forest Fire rate is pressure dependent, these overshoots may have a substantial effect on the tendency of a detonation to fail. The 2DE input instruction manual recommends artificial viscosity coefficients between 0.001 and 0.1 with lower values preferred! These values are quite low and generally produce significant overshoots. We ran computations of detonation propagation using Forest Fire in cylindrical Composition B charges with various viscosity coefficients. Square zones, which are essential when viscous shocks are present, were employed. The detonation pressures produced are summarized in Table A-1. The nominal Chapman-Jouget pressure for Composition B is 29.5 GPa. Therefore, an artificial viscosity coefficient of 1.5 was used in all reported computations.

Table A-1. Effect of Artificial Viscosity on Detonation Pressure

Viscosity Coefficient	Detonation Pressure (GPa)
0.01	50
0.10	45
0.50	37
1.00	34
1.50	31

CONVERGENCE

The stability of the solutions obtained depend on the computational zone size used. Solutions are expected to converge as the zone size gets smaller. However, Lundstrom (1993)† did not observe such convergence in his computations using a modified version of Forest Fire. We determined the failure radius of Composition B in computations with zone sizes ranging from 0.0125 to 0.1000 mm square. For

---

† Lundstrom, E. A. "A Numerical Study of Fragment Impact on Bare Explosive." Proceedings of the 1993 JANNAF Propulsion Systems Hazards Subcomittee Meeting, 1993.

cast TNT, we used zone sizes ranging from 0.250 to 1.000 mm square. The results are summarized in Table A-2. In each case, detonation failure occurred at the smaller of the two radii given while propagation occurred at the larger. We have plotted the results for Composition B along with those of Lundstrom in Figure A-1. We did not observe the rapid divergence of the solution with decreasing zone size that he did. Our results are substantially the same for all but the coarsest zoning. For TNT the results drift slowly toward smaller failure radii as the zone size decreases. Based on these results, zone sizes of 0.050 mm for Composition B and 0.500 mm for cast TNT were used in all reported computations.

Table A-2. Effect of Zone Size on Failure Diameter

Composition B		Cast TNT	
Zone Size (mm)	Failure Radius (mm)	Zone Size (mm)	Failure Radius (mm)
0.0125	2.0–2.1	—	—
0.0250	2.0–2.2	0.250	14.0–15.0
0.0333	2.0–2.2	0.333	15.0–16.0
0.0500	2.1–2.2	0.500	16.0–17.0
0.1000	2.5–3.0	1.000	21.0–22.0

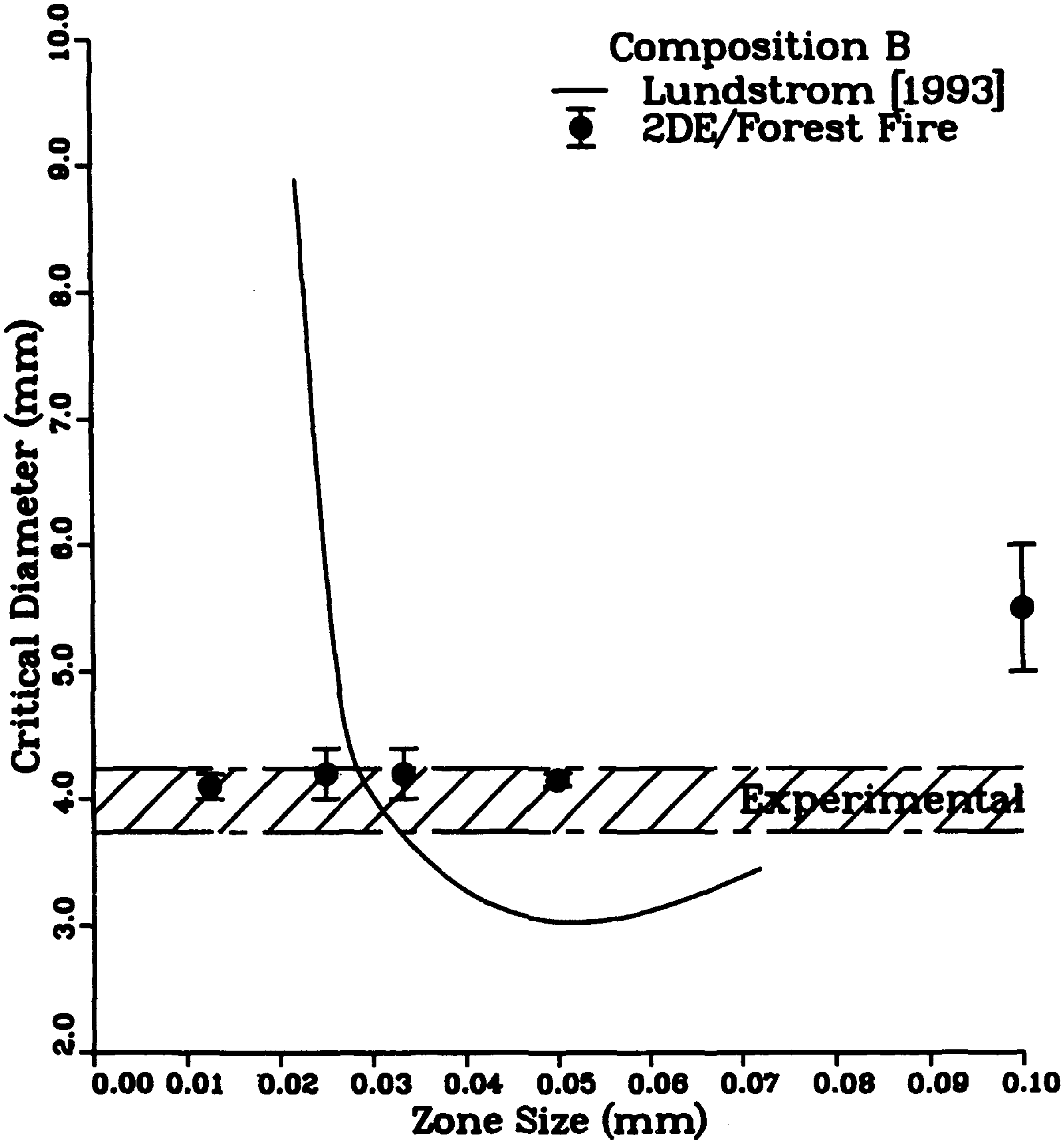

Figure A-1. Convergence of failure diameter solutions for Composition B as a function of zone size.

INTENTIONALLY LEFT BLANK.

NO. OF COPIES	ORGANIZATION
2	ADMINISTRATOR DEFENSE TECHNICAL INFO CENTER ATTN: DTIC-DDA CAMERON STATION ALEXANDRIA VA 22304-6145
1	COMMANDER US ARMY MATERIEL COMMAND ATTN: AMCAM 5001 EISENHOWER AVE ALEXANDRIA VA 22333-0001
1	DIRECTOR US ARMY RESEARCH LABORATORY ATTN: AMSRL-OP-SD-TA/ RECORDS MANAGEMENT 2800 POWDER MILL RD ADELPHI MD 20783-1145
3	DIRECTOR US ARMY RESEARCH LABORATORY ATTN: AMSRL-OP-SD-TL/ TECHNICAL LIBRARY 2800 POWDER MILL RD ADELPHI MD 20783-1145
1	DIRECTOR US ARMY RESEARCH LABORATORY ATTN: AMSRL-OP-SD-TP/ TECH PUBLISHING BRANCH 2800 POWDER MILL RD ADELPHI MD 20783-1145
2	COMMANDER US ARMY ARDEC ATTN: SMCAR-TDC PICATINNY ARSENAL NJ 07806-5000
1	DIRECTOR BENET LABORATORIES ATTN: SMCAR-CCB-TL WATERVLIET NY 12189-4050
1	DIRECTOR US ARMY ADVANCED SYSTEMS RESEARCH AND ANALYSIS OFFICE ATTN: AMSAT-R-NR/MS 219-1 AMES RESEARCH CENTER MOFFETT FIELD CA 94035-1000

NO. OF COPIES	ORGANIZATION
1	COMMANDER US ARMY MISSILE COMMAND ATTN: AMSMI-RD-CS-R (DOC) REDSTONE ARSENAL AL 35898-5010
1	COMMANDER US ARMY TANK-AUTOMOTIVE COMMAND ATTN: AMSTA-JSK (ARMOR ENG BR) WARREN MI 48397-5000
1	DIRECTOR US ARMY TRADOC ANALYSIS COMMAND ATTN: ATRC-WSR WSMR NM 88002-5502
1	COMMANDANT US ARMY INFANTRY SCHOOL ATTN: ATSH-WCB-O FORT BENNING GA 31905-5000
	ABERDEEN PROVING GROUND
2	DIR, USAMSAA ATTN: AMXSY-D AMXSY-MP/H COHEN
1	CDR, USATECOM ATTN: AMSTE-TC
1	DIR, USAERDEC ATTN: SCBRD-RT
1	CDR, USACBDCOM ATTN: AMSCB-CII
1	DIR, USARL ATTN: AMSRL-SL-I
5	DIR, USARL ATTN: AMSRL-OP-AP-L

NO. OF COPIES	ORGANIZATION
1	HQDA (SARD-TT/DR. F MILTON) WASH DC 20310-0103
1	HQDA (SARD-TT/MR J APPEL) WASH DC 20310-0103
8	LOS ALAMOS NATIONAL LABORATORY ATTN: BLAINE W ASAY ALAN L BOWMAN CHARLES A FOREST JAMES E KENNEDY EDWARD M KOBER PIER K TANG JOHN B RAMSAY JERRY WACKERLE LOS ALAMOS NM 87545
2	LOS ALAMOS NATIONAL LABORATORY ATTN: JOHN C DALLMAN PHILIP M HOWE PO BOX 1663 LOS ALAMOS NM 87545
1	LOS ALAMOS NATIONAL LABORATORY ATTN: WILLIAM C DAVIS 693 46TH STREET LOS ALAMOS NM 87545
4	LAWRENCE LIVERMORE NATIONAL LAB ATTN: MILTON FINGER MICHAEL J MURPHY CRAIG M TARVER PO BOX 808 LIVERMORE CA 94550
3	SANDIA NATIONAL LABORATORY ATTN: MELVIN R BAER GERRY I KERLEY ROBERT E SETCHELL PO BOX 5800 ALBUQUERQUE NM 87185-5800
4	NAVAL SURFACE WARFARE CENTER ATTN: RICHARD R BERNECKER KIBONG KIM LESLIE A ROSLUND HAROLD W SANDUSKY 10901 NEW HAMPSHIRE AVENUE SILVER SPRING MD 20903-5640
2	US ARMY ARDEC ATTN: BARRY D FISHBURN VLADIMIR M GOLD PICATINNY ARSENAL NJ 07806-5000
1	DYNA EAST CORPORATION ATTN: PEI CHI CHOU 3201 ARCH STREET PHILADELPHIA PA 19104
1	VANDERBILT UNIVERSITY ATTN: ARTHUR M MELLOR BOX 1592 NASHVILLE TN 37235-1592
1	NEW MEXICO INSTITUTE OF MINING TECHNOLOGY ATTN: LARRY D LIBERSKY CAMPUS STATION SOCORRO NM 87801
1	GRYTING ENERGETICS SCIENCE COMPANY ATTN: HAROLD J GRYTING 7126 SHADOW RUN SAN ANTONIO TX 78250-3483
1	SRI INTERNATIONAL ATTN: MICHAEL COWPERTHWAITE 333 RAVENSWOOD AVENUE MENLO PARK CA 94025
1	WRIGHT LABORATORY ATTN: J GREGORY GLENN ARMAMENT DIRECTORATE EGLIN AFB FL 32542-5434
	ABERDEEN PROVING GROUND
12	DIR, USARL ATTN: AMSRL-WT-TB/ ROBERT B FREY ONA R LYMAN JERRY L WATSON FREDERICK H GREGORY VINCENT M BOYLE WARREN W HILLSTROM EVELYN A MCDOUGAL WILLIAM LAWRENCE KELLY J BENJAMIN TONI M DORSEY AMSRL-WT-T/WALTER F MORRISON AMSRL-WT-TA/JAMES T DEHN

NO. OF COPIES	ORGANIZATION
1	DGA/CENTRE D'ETUDES DE GRAMAT ATTN: DIDIER BERGUES GRAMAT, 46500, FRANCE
1	ICI EXPLOSIVES ATTN: DAVID L KENNEDY PO BOX 196 GEORGE BOOTH DRIVE NEW SOUTH WALES, 2327, AUSTRALIA
1	AGENCY FOR DEFENSE DEVLOPMENT ATTN: JAIMIN LEE YUSEONG PO BOX 34 (1-3-7) TAEJON, 305-600, KOREA
1	COMMISSARIAT A L'ENERGIE ATOMIQUE ATTN: JEAN-PAUL PLOTARD COURTRY, 77181, FRANCE
2	FRENCH-GERMAN RESEARCH INSTITUTE ATTN: HENRY P A MOULARD MICHEL M S SAMIRANT 5 RUE DE GENERAL CASSAGNOU SAINT-LOUIS CEDEX, 68301, FRANCE
1	DEFENCE RESEARCH ESTABLISHMENT, VALCARTIER ATTN: CONRAD BELANGER 2459 PIE XI BOULEVARD NORTH QUEBEC, GOA 1RO, CANADA
1	DEFENCE RESEARCH AGENCY ATTN: PETER J HASKINS FORT HALSTEAD SEVENOAKS, KENT TN14 7BP ENGLAND
1	ATOMIC WEAPONS ESTABLISHMENT (FOULNESS) ATTN: HUGH R JAMES FOULNESS ISLAND SOUTHEND-ON-SEA, ESSEX, SS3 9XE ENGLAND

INTENTIONALLY LEFT BLANK.

USER EVALUATION SHEET/CHANGE OF ADDRESS

This Laboratory undertakes a continuing effort to improve the quality of the reports it publishes. Your comments/answers to the items/questions below will aid us in our efforts.

1. ARL Report Number ARL-TR-616 Date of Report November 1994

2. Date Report Received ______

3. Does this report satisfy a need? (Comment on purpose, related project, or other area of interest for which the report will be used.) ______

4. Specifically, how is the report being used? (Information source, design data, procedure, source of ideas, etc.) ______

5. Has the information in this report led to any quantitative savings as far as man-hours or dollars saved, operating costs avoided, or efficiencies achieved, etc? If so, please elaborate. ______

6. General Comments. What do you think should be changed to improve future reports? (Indicate changes to organization, technical content, format, etc.) ______

CURRENT ADDRESS

Organization

Name

Street or P.O. Box No.

City, State, Zip Code

7. If indicating a Change of Address or Address Correction, please provide the Current or Correct address above and the Old or Incorrect address below.

OLD ADDRESS

Organization

Name

Street or P.O. Box No.

City, State, Zip Code

(Remove this sheet, fold as indicated, tape closed, and mail.)
(DO NOT STAPLE)

DEPARTMENT OF THE ARMY

OFFICIAL BUSINESS

NO POSTAGE
NECESSARY
IF MAILED
IN THE
UNITED STATES

BUSINESS REPLY MAIL
FIRST CLASS PERMIT NO 0001, APG, MD

Postage will be paid by addressee

Director
U.S. Army Research Laboratory
ATTN: AMSRL-OP-AP-L
Aberdeen Proving Ground, MD 21005-5066